Journal of Applied Mechanics and Technical Physics, Vol. 44, No. 2, pp. 262–270, 2003

PLASTIC FLOW LOCALIZATION IN COMMERCIAL ZIRCONIUM ALLOYS

T. M. Poletika, G. N. Narimanov, S. V. Kolosov, and L. B. Zuev

UDC 660.539.382.2

The behavior of plastic flow curves and patterns of plastic strain localization were studied for tension of samples of Zr–1% Nb (É110 *alloy) and* Zr–1% Nb-1.3% Sn–0.4% Fe (É635 *alloy) were studied. The relationship of the localization kinetics with the strain hardening law in plastic flow and transition to fracture is established. The dislocation microstructure of the alloys in strain localization and prefracture zones is examined.*

Key words: *strain hardening, plastic flow, localization, dislocation structure.*

Introduction. The experimental data accumulated to date indicate that plastic flow localization occurs at all loading stages [1, 2]. The plastic flow regime on a given segment of a strain curve was found to be uniquely related to the type of time–space distribution of the plastic-distortion tensor components. It was shown that the capability of materials for plastic distortion can be judged from macropatterns of strain localization, for example, in cold working by pressure [3].

In the present work, we studied strain localization in samples of commercial É110 and É635 zirconium alloys used in the manufacture of fuel element tubes for nuclear reactors [4, 5]. Unlike in previous studies [6, 7], in the present paper, focus is on the final deformation stage preceding necking. Interest in Zr alloys with a hexagonal close-packed lattice is due to the fact that their deformation and plastic flow curves have been poorly studied. There is no unified concept on the nature of plastic strain and the mechanisms of strain hardening even for pure zirconium [8–10]. As regards multicomponent zirconium-based alloys, their strain characteristics and capability for plastic distortion are largely determined by the complex phase composition and microstructure of the material. Therefore, studies of plastic flow localization processes corresponding to various stages on strain curves up to fracture and their correlation with changes in the microstructure are very urgent. These data are required to clarify special features in the evolution of the microstructure that lead to strain localization at the macrolevel and formation of a fracture site, in particular, to estimate the technological plasticity margin of É110 and É635 alloys.

Materials and Experimental Technique. Zr–1% Nb (É110) and Zr–1% Nb–1.3% Sn–0.4% Fe (É635) alloys were used. É110 alloy consisted of recrystallized α-Zr grains (mean grain size about 5 μm) with β-Nb inclusions with a size of up to 0.08 μm. É635 alloy consisted of recrystallized 4 μm size grains of α-Zr with dispersed inclusions of Fe_2Zr, Nb_2Zr, and Zr_3Fe intermetallides with a size about 0.08 μm inside the grains and on their boundaries [11].

Flat samples with working-section dimensions of $42 \times 5 \times 2$ mm were extended on an Instron-1185 machine at a rate of displacement of the moving clump of 0.1 mm/min ($\dot{\varepsilon} = 4 \cdot 10^{-5}$ sec^{-1}). The field of point displacement vectors on the sample surface $\boldsymbol{r}(x, y)$ was recorded simultaneously with recording stress–strain curves by speckle interferometry [2, 12], we recorded Apparently, all components of the plastic distortion tensor $\beta_{i,j} = \nabla \boldsymbol{r}$ can be obtained by differentiation of this field. Below, we give distributions of just one components — local strain $\varepsilon_{xx} = \partial u/\partial x$ (u is the projection of the $\boldsymbol{r}$ vector onto the tension axis x).

Institute of Strength Physics and Materials Science, Siberian Division, Russian Academy of Sciences, Tomsk 634021. Translated from Prikladnaya Mekhanika i Tekhnicheskaya Fizika, Vol. 44, No. 2, pp. 132–142, March–April, 2003. Original article submitted December 11, 2002.

 0021-8944/03/4402-0262 $25.00

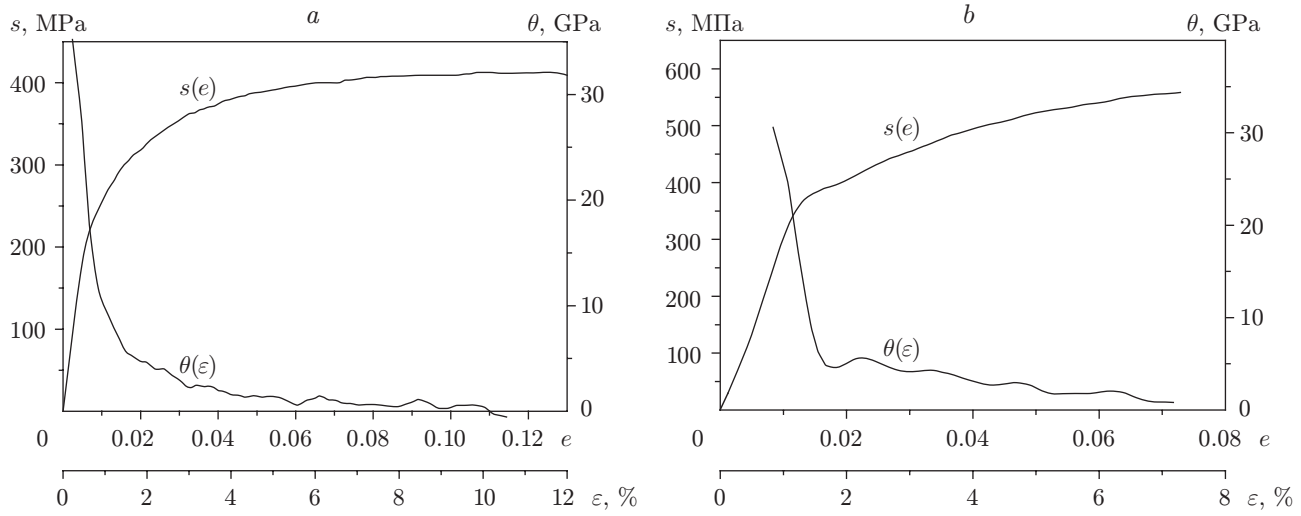

Fig. 1

Because of the high plasticity of É110 and É635 alloys, their strain curves and curves of the strain hardening coefficient ($\theta = ds/de$) versus strain were analyzed after transition from conditional stresses σ and strains ε to true stresses $s = \sigma(1 + \varepsilon)$ and strains $e = \ln(1 + \varepsilon)$.

Various stages on plastic flow curves are easily revealed by plotting the curves in the coordinates $\ln(s - s_e)$–$\ln e$, where $s_e = \sigma_e(1 + \varepsilon_e)$. The quantity σ_e is determined by extrapolating the curve of $\sigma(\varepsilon)$ in the coordinates s–$\sqrt{e}$ [13] into the neighborhood of $\varepsilon = 0$. In the coordinates $\ln(s - s_e)$–$\ln e$, the parabola $s \sim e^n$ becomes a straight line with a slope $n = d[\ln(s - s_e)]/d(\ln e)$, which is a natural flow characteristic.

Electron-microscopic studies were performed on an ÉVM–125K electron microscope at an accelerating voltage equal to 125 kV using thin foils prepared by electropolishing in an 90% CH_3OH + 10% $HClO_4$ electrolyte at a temperature of −50°C.

Experimental Results. The loading curves of the examined alloys are similar to one another (Fig. 1). On these curves, there is a transitional hardening stage, which follows immediately after the yield point, and a parabolic hardening law is satisfied. However, for É110 alloy (Fig. 1a), the transitional stage with decreasing strain hardening coefficient is followed by a short linear stage (in this stage, the strain increases by not more than 0.5%, $\theta \approx 6$ GPa), whereas for É635 alloy (Fig. 1b), the transitional stage is followed by bending of the strain curve. According to the data of [14], similar segments, called yield areas, were observed in zirconium and its alloys. In particular, such an area of a rather great extension was observed in Zircaloy-4 [15]. For zirconium alloys, its occurrence is explained by the pinning of dislocations by Cottrell atmospheres of oxygen atoms (interstitial impurity in Zr) and by O–O or O–S pairs (O is oxygen and S is a substitutional impurity) [16]. On the strain curve of É635 alloy, the yield area with a length of approximately 0.2% and a constant strain hardening coefficient $\theta \approx 4$ GPa is followed by a transitional stage, at which the values of θ increase (Fig. 1b).

For both alloys, the parabolic hardening stage begins at $\varepsilon \approx 2\%$ and is characterized by a constantly decreasing coefficient θ (Fig. 1). Beginning with $\varepsilon \approx 5\%$, the coefficient θ becomes very small and then close to zero, which corresponds to the fourth stage of strain hardening [17].

The use of the logarithmic coordinates $\ln(s - s_e)$–$\ln e$ allows each parabolic strain curve to be divided into five straight-line segments with a constantly decreasing parabolicity factor n (Fig. 2). In the case of É635 alloy, the value of n runs over values of 0.54, 0.49, 0.4, 0.3, and 0.2 (curve 1) and in the case of É110 alloy, it runs over values of 0.7, 0.5, 0.4, 0.25, and 0.2 (curve 2). The transitions between the segments of the parabolic curve have different lengths; the transition between the third and fourth segments (with $\varepsilon \approx 5\%$ for É635 alloy and ≈6% for É110 alloy) has the greatest length equal to 0.2% and a nearly zero slope.

The plastic flow curve is terminated by a segment with $n \approx 0$, which corresponds to the stage of development of a visible neck (not shown in Fig. 2) The total length of the parabolic stage before this moment is 12% for É110 alloy and 9% for É635 alloy. The greater elongation of recrystallized É110 alloy before fracture compared to É635 alloy is accompanied by an about two-fold decrease in the yield point and tensile strength. The difference in mechanical properties is due to different doping of the alloys.

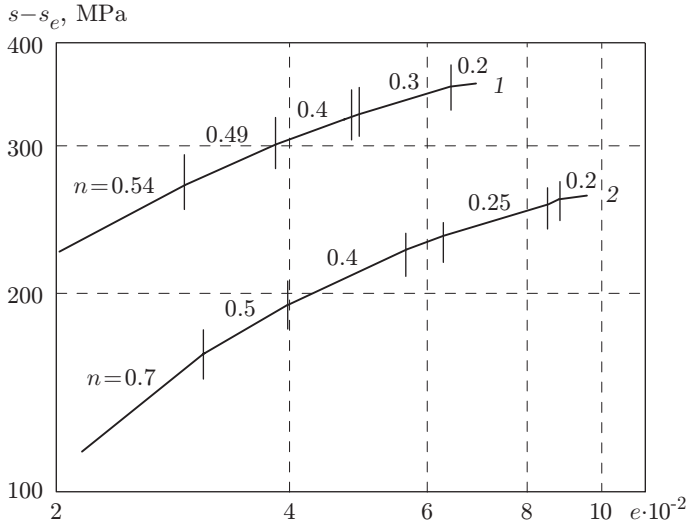

Fig. 2

As is known, the stages on the plastic flow curve are related to the plastic strain localization patterns [1, 2]. This is also valid for the examined Zr alloys. The evolution of the macrolocalization pattern of strains ε_{xx} at all stages of the strain curve was traced using laser speckle interferometry. Thus, for É110 alloy, motion of local elongation maxima is observed on the initial segment of the stress–strain curve corresponding to the transitional stage and at the linear stage. As regards É635 alloy, an analysis of the strain localization patterns in the neighborhood of the yield point shows that one strain localization font originates at $\varepsilon = 1\%$ [which corresponds to the inflection on the s–e curve (Fig. 1b)]. This front contains almost the entire strain of the sample ($\varepsilon = 1\%$), as in the case of strain localization in an yield area in Luders bands. Behind this front, which propagates at a velocity of about $1.4 \cdot 10^{-5}$ m/sec, other, less intense, local elongation maxima originate and move. The development of strain localization in the interval $1.03\% < \varepsilon < 1.82\%$ for É635 alloy is shown in Fig. 3. The scale corresponds to local strain values ε_{xx}.

For $\varepsilon \approx 2\%$, plastic deformation covers the entire sample and a stationary (fixed) system of localization maxima is established that corresponds to the parabolic stage of plastic flow [1, 2]. Figure 4a and b shows the local strain distribution for É635 alloy in the parabolic stage of strain hardening with $n \approx 0.5$ and in the prefracture stage with $n \to 0$, respectively. The scale corresponds to local strain values ε_{xx}. Thus, in the transitional stage of the strain curve with an increasing strain hardening coefficient, a stationary system of localized strain nuclei is formed.

For É110 alloy, a stationary system of local elongation maxima arises after transition to the parabola segment with $n \approx 0.7$. Motion of the localized strain maxima begins from $n < 0.5$ and continues on segments with smaller parabolicity factors until necking. Figure 5a gives a curve of the localization maxima (x is the abscissa of the localized strain nucleus on the sample axis) versus the total strain of the É110 sample.

For É635 alloy, a stationary system of localized strain nuclei (Fig. 5b) is also observed on the first two segments with parabolicity factors $n = 0.54$ and 0.49. Despite the close values of n, the positions of the maxima differ because the stationary system is shifted in the range $\varepsilon = 2.8$–3.2%. Next, as in the case of É110 alloy, motion of strain localization fronts starts on the segment of the parabolic curve with $n < 0.5$ and continues until necking (Fig. 5b).

Microstructure of the Deformed Material. Electron-microscopic studies of the structure of deformed samples were conducted until a total strain $\varepsilon = 1.8$ and 7.7% was attained for É635 alloy and $\varepsilon = 7\%$ for É110 alloy.

Speckle interferometry studies showed that the deformation of the É635 sample from the moment of the yield point to the beginning of the parabolic stage ($\varepsilon \approx 2\%$) is due to the motion of the principal strain localization maximum followed by less intense maxima) (see Fig. 3). After cessation of tension at a strain $\varepsilon = 1.8\%$, the values of the increments of ε_{xx} were summed up and the position of the strain localization front was determined.

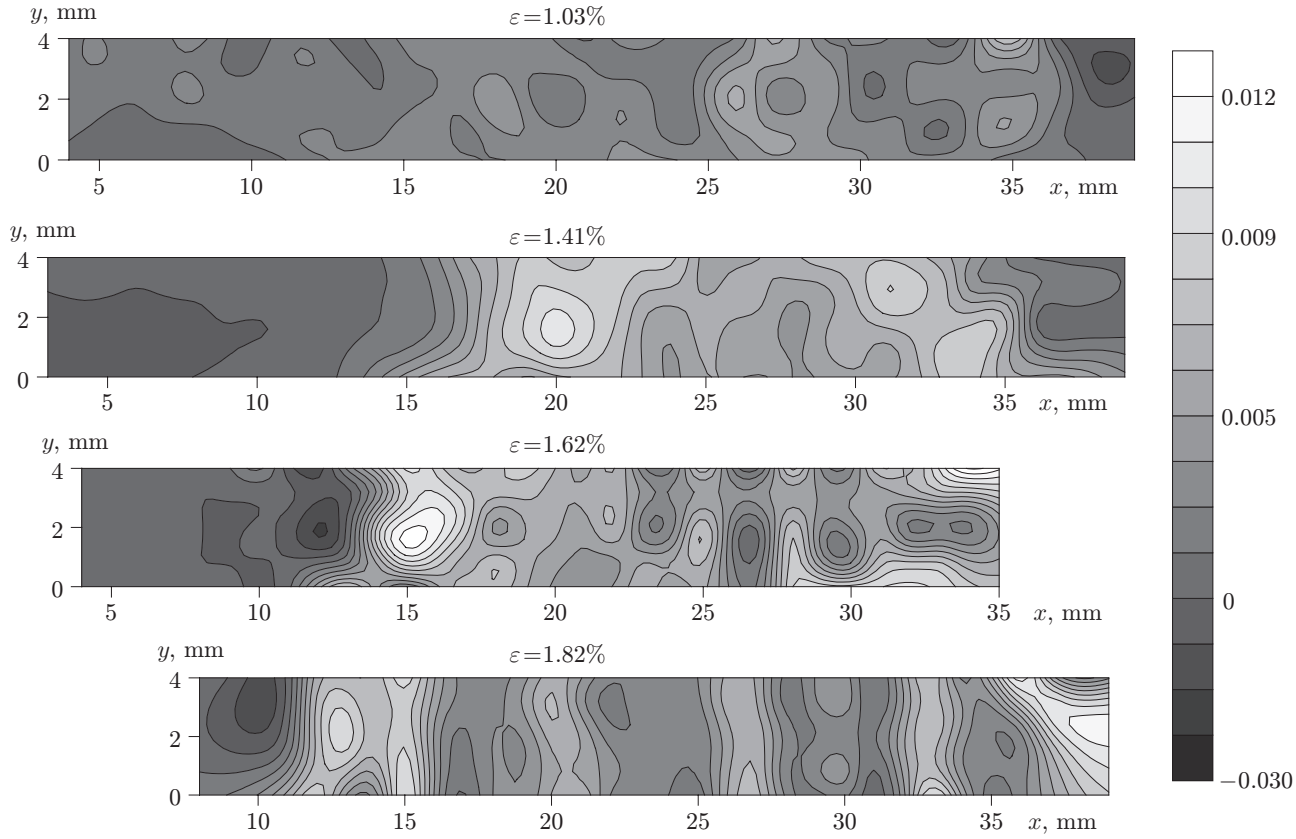

Fig. 3

Foils for the electron-microscopic studies were cut out from two regions: 1) ahead of the strain localization front ($\varepsilon_{xx} \approx 0$); 2) inside the localized strain nucleus ($\varepsilon_{xx} > 10^{-2}$). In region 1 a random distribution of nearly noninteracting dislocations (long single dislocations and dislocation clusters, arrays, and sometimes aggregations) observed (Fig. 6a). Such a microstructure is characteristic of the transitional stage following the yield point in polycrystals, in which the strain hardening coefficient decreases [13]. In region 2, a network dislocation structure is predominantly observed. Its formation begins near the grain boundaries (Fig. 6b). The nodes of the dislocation network are pinned by particles of the second phase, and in some segments of the network structure, particles lie on dislocations, i.e., are interrelated. The formation of the network structure corresponds to the transitional stage [17] characterized by an increase in the strain hardening coefficient.

After the attainment of a total strain $\varepsilon \approx 7.7\%$, the samples were cut in the region of the localization maximum and in its neighborhood, in which the strain value is much less. Figure 7a shows a streaky structure typical of the segment with $n \approx 0.2$; a cellular-network dislocation substructure with a high dislocation density is observed between the boundaries of the streaks. The microstructure of the alloy in the neighborhood of the strain localization maximum is given in Fig. 7b. Further development of the streaky structure is observed. As a result, the crystallographic orientation of the streaky substructure is disturbed and the microstreaks are separated into segments with a partly fragmented structure and a substructure with multidimensional discrete and continuous disorientations. On electron diffraction patterns, the azimuthal disorientation of such areas reach 20°; the electron diffraction patterns contain arcs of point reflections, indicating a high dispersity of the structure (Fig. 7b). It is known that the formation of substructures with multidimensional discrete and continuous disorientations are characteristic of the fourth stage of deformation [17].

In [6, 7], it is established that on parabolic curve segments with $n < 0.5$, the plastic deformation of recrystallized É110 alloy develops with the formation of cellular-network and streaky substructures and with the formation of a substructure with multidimensional disorientations. In the neighborhood of the prefracture site, the formation of a fragmented structure is possible. In the present paper, we compare the dislocation structure of alloy É635 with

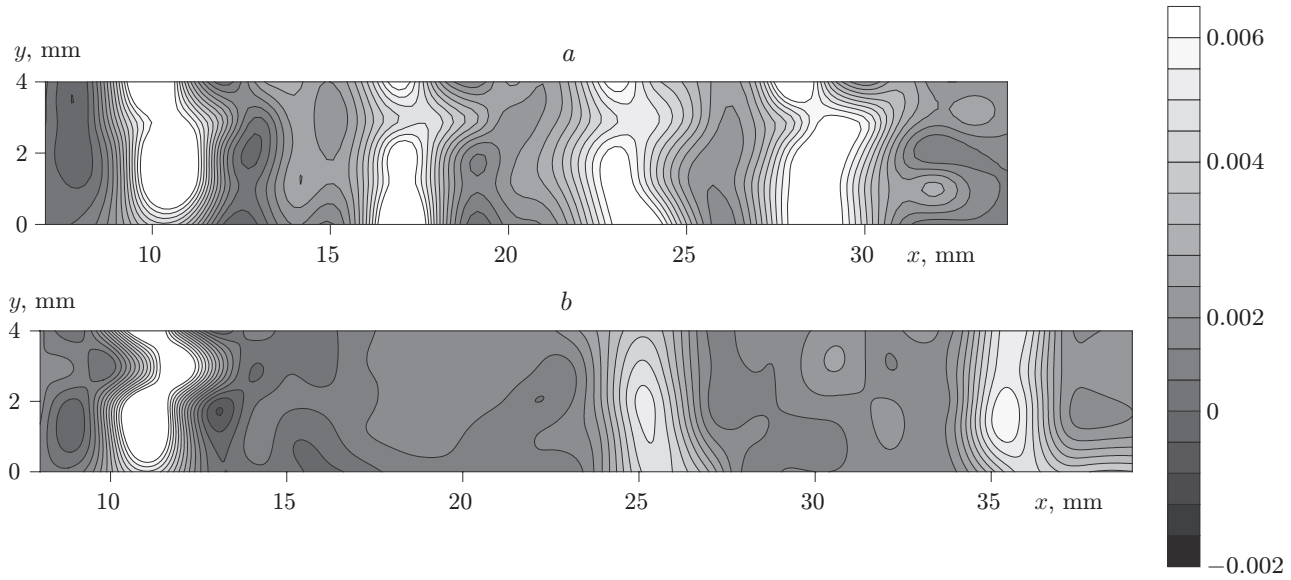
y, mm
a
4
2
0
10
15
20
25
30
x, mm
y, mm
b
4
2
0
10
15
20
25
30
35
x, mm
0.006
0.004
0.002
0
−0.002

Fig. 4

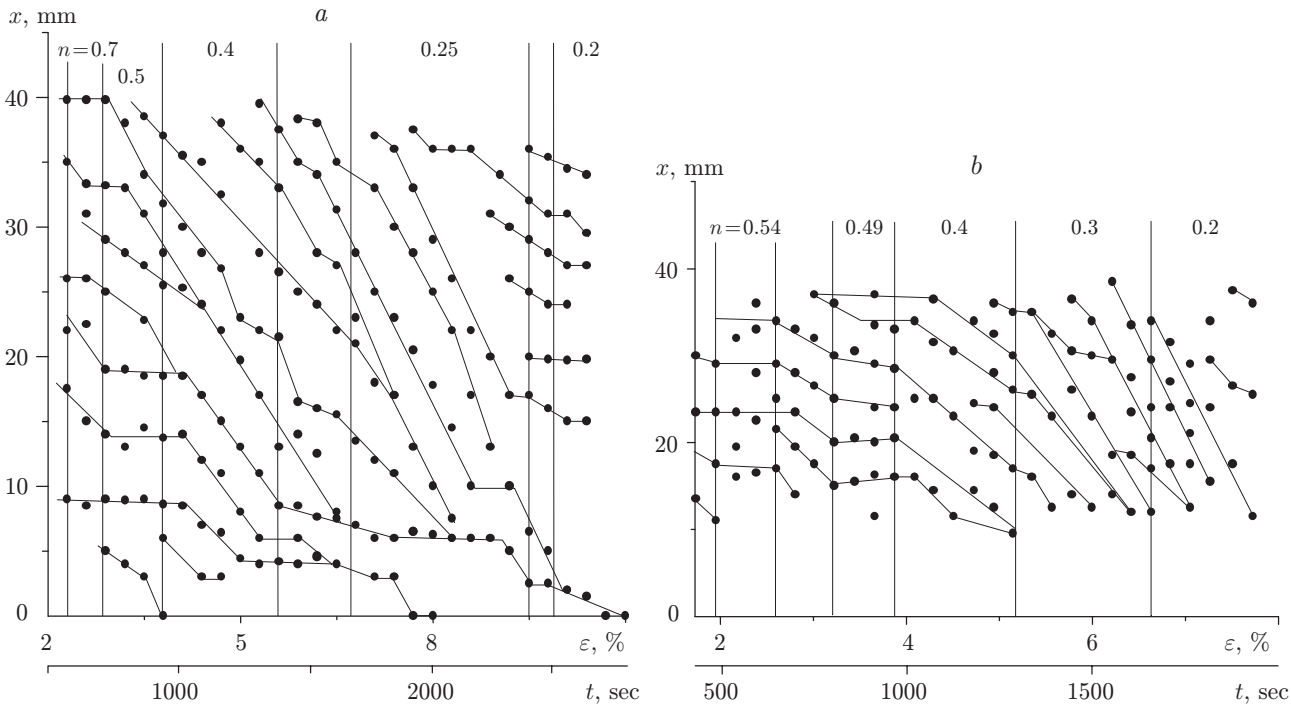
x, mm
a
n=0.7
0.5
0.4
0.25
0.2
40
30
20
10
0
2
5
8
ε, %
1000
2000
t, sec
x, mm
b
n=0.54
0.49
0.4
0.3
0.2
40
20
0
2
4
6
ε, %
500
1000
1500
t, sec

Fig. 5

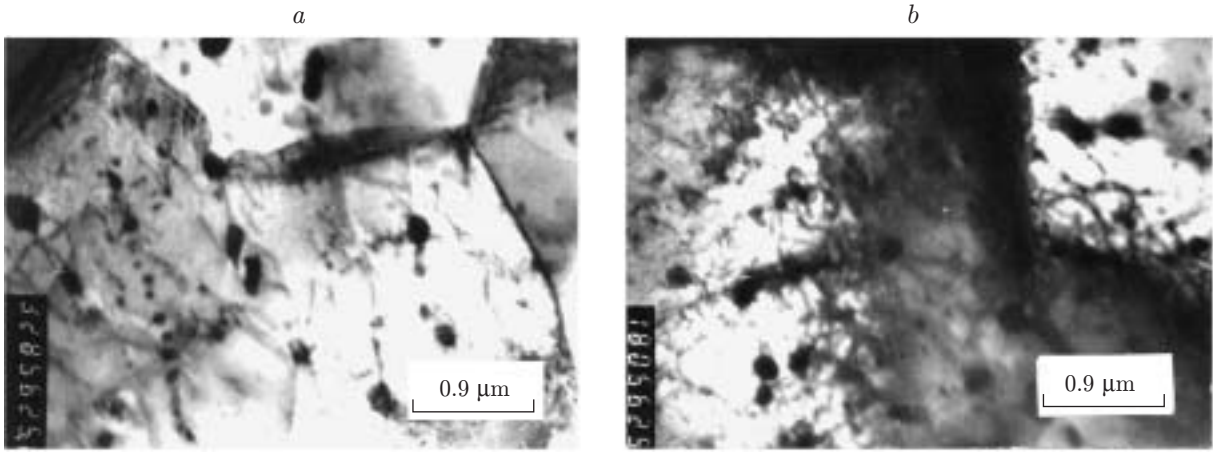

Fig. 6

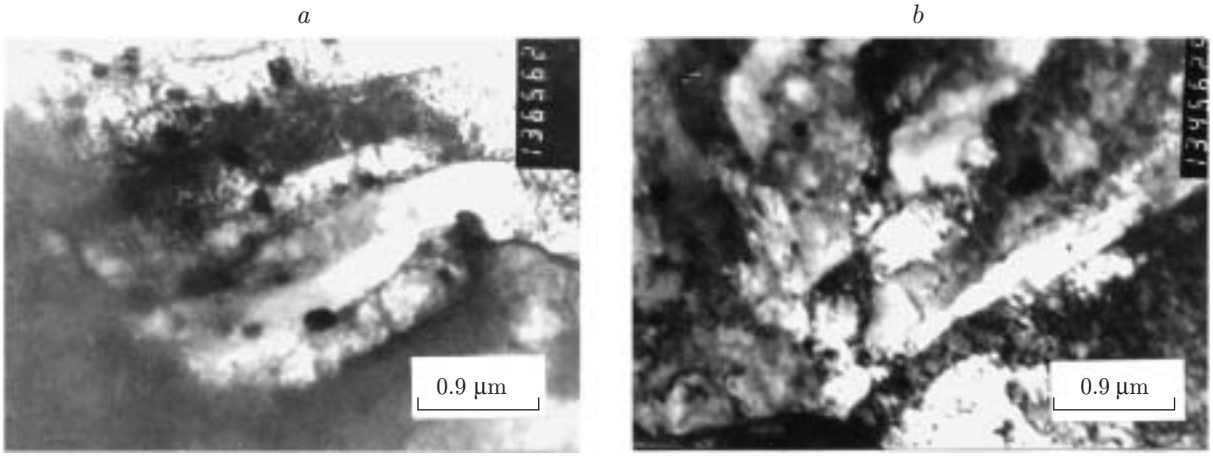

Fig. 7

the dislocation structure of alloy É110, strained to a value $\varepsilon = 7\%$ ($n \approx 0.2$). Figure 8 shows the microstructures of the alloy in the neighborhood of the strain localization maximum, in which a neck is then formed, and in the neighborhood of the local elongation minimum. In the neighborhood of the minimum (Fig. 8a), a streaky substructure is observed. Inside separate streaks, elements of the cellular–network dislocation substructure typical of the previous deformation stage are discernible with azimuthal disorientations on the subboundaries equal to 1–3°. In the neighborhood of the strain localization maximum, fragments with an azimuthal disorientation of 5° (Fig. 8b) appear along with the substructure containing multidimensional disorientations. The data obtained correspond to the model proposed in [18], according to which neck strain develops owing to a gradual increase in the disorientation of neighboring elements of the substructure. Our experiments showed that by the moment of fracture, a fragmented substructure with large-angle boundaries formed in both alloys.

The presence of grain boundaries, dispersed particles, and impurities accelerates the formation of each subsequent dislocation substructure due to the higher dislocation density. At the moment necking begins, the degree of preparedness to form a fragmented structure is higher for such alloys. This means that substructures in such material change faster. Apparently, the complex (compared to É110 alloy) microstructure of alloy É635 is responsible for the higher rate of motion of the localized strain nuclei on the segments with a parabolicity factor $n < 0.5$ (see Fig. 5).

A comparison of electron-microscopic results with data on the evolution of strain localization at the parabolic stage ($n < 0.4$) leads to the conclusion that the fourth stage of the plastic flow, at which $n \to 0$, is due to the formation of a prefracture site necking in the material.

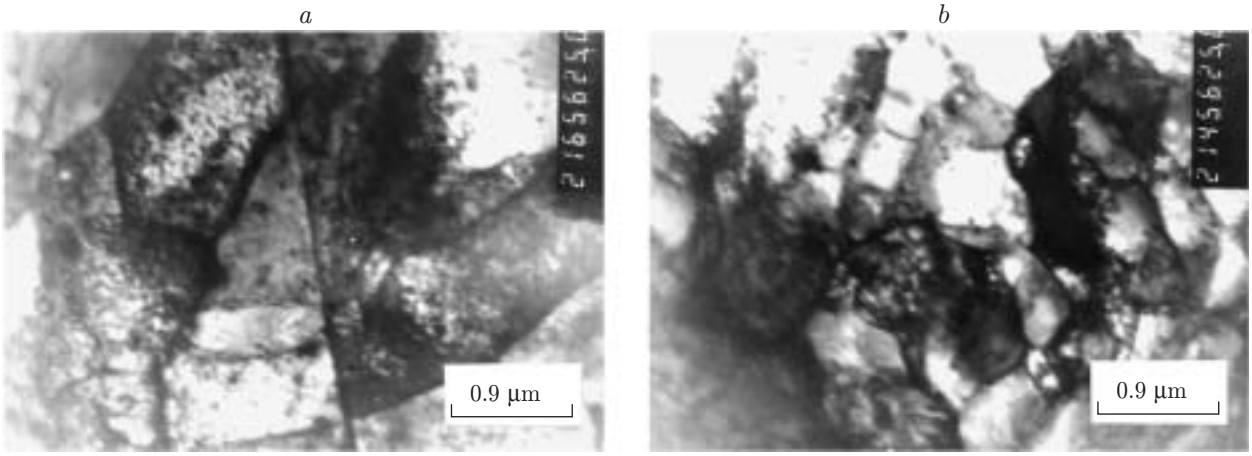

Fig. 8

Results and Discussion. An analysis of the dependence of ε_{xx} on the total strain showed that the strain localization fronts move toward the necking site. From Fig. 5 it follows that the first intense strain localization maximum at the necking site occurs in both alloys at the end of the parabolic curve segment with a factor $n \approx 0.5$. Apparently, this strain localization maximum can be considered a precursor of the formation of a fracture site. The motion of the localization fronts on the next segment is directed toward the prefracture site and is apparently due to the formation of this site: the strain maxima "travel" the entire sample, and strain is accumulated in the place of formation of the primary prefracture site. For example, for alloy É635 with $n \approx 0.4$, the time of complete "travel" is about 360 sec, and the period of strain accumulation in the sample is 100 sec; for É110 alloy, these values are about 550 and 200 sec, respectively. On the segment with $n \approx 0.3$, new strain localization fronts originate in place of the maxima that have moved toward the necks, and the process is repeated but the rate of motion of local elongation maxima is higher (see Fig. 5).

Between the parabolic segments of the strain curve with factors $n \approx 0.4$ and ≈ 0.3 there is an almost horizontal segment, on which the strain increases by 0.2%. This segment corresponds to the moment of formation of a primary neck. The strain localization corresponding to the present moment is shown in Fig. 4b (there is a region in which the strain maximum far exceeds the strain maxima in the remaining localization nuclei).

On the segment of the parabolic stage of strain hardening with a parabolicity factor $n \approx 0.2$, the formation of a prefracture site is nearly completed. On the next segment with $n \to 0$ there is formation of a neck, which is already visible at this moment.

Figure 9 presents curves of the velocity v of motion of the localized strain fronts at the parabolic hardening stage versus the parabolicity factor n for É635 (curve 1) and É110 alloys in the recrystallized (curve 2) and quenched (curve 3) states. The tensile strengths σ_t of the alloys in these states were 580, 440, and 330 MPa, respectively. It should be noted that an increase in the σ_t of the examined alloys leads to an increase in the velocities of the localized strain nuclei. This indicates that the velocity of propagation of the strain localization fronts toward the neck, i.e., the rate of necking, is determined by the stress level in the sample under plastic flow.

One of the most important features of the plastic flow localization, which is detected for the first time in the experiments performed, is the motion of local strain nuclei toward one of them with a parabolicity factor $n < 0.5$. The difference in the location and motion of nuclei with, e.g., $n = 1/2$ ($\varepsilon \sim \sigma^2$) and $1/3$ ($\varepsilon \sim \sigma^3$), can caused by the following factors. If the local stresses change randomly by $\pm\delta\sigma$ at the leading and rear edges of the strain nucleus, the symmetric strain distribution is retained in the former case and is disturbed in the second case, resulting in displacement of the localized plastic nucleus.

A generalized curve of the velocity of the localized strain nuclei v versus the parabolicity factor n for recrystallized É110 alloy is given in Fig. 10 (points correspond to experimental data). From the equation of this curve $v = 2.63 \cdot 10^{-4}(n - 0.64)^2$ it follows that the localized strain nucleus form a stationary structure only for n close to the value predicted by the Taylor–Mott strain hardening model [19], i.e., for $n \approx 0.5$.

As shown by the data given above, for $n < 0.5$, the localized flow nuclei unite, resulting in necking and transition from plastic flow to plastic fracture. In this case, the localized strain nuclei move but their motion is not

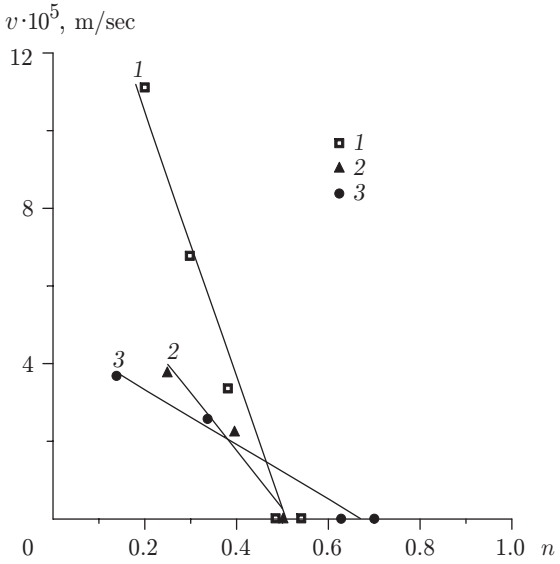

Fig. 9

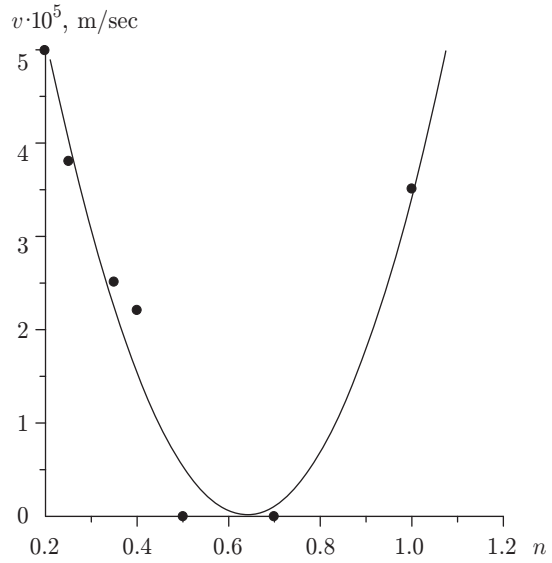

Fig. 10

consistent, unlike in the stage of linear hardening [1, 2]. There is an analogy between the motion of the localized strain nuclei and the motion of combustion nuclei in a nonlinear medium [20] during their coalescence into a single zone surrounded by an inactive region. The reason of such coalescence in combustion lies in the exchange of thermal energy between neighboring nuclei in a medium with nonlinear thermal conductivity. In the case of coalescence of plastic strain nuclei, there is also an exchange of elastic energy between neighboring nuclei due to acoustic pulses (see, e.g., [21]).

Conclusions. It is established that the plastic flow curves of recrystallized É110 and É635 zirconium alloys are multistage and the parabolic stage include five segments on which the parabolicity factor decreases.

Distributions of the fronts of local elongations ε_{xx} at each stage of the loading curve up to necking were obtained by laser speckle interferometry. These data were used to study the necking kinetics in zirconium alloys of different composition and structure. It is established that the velocity of propagation of the strain localization fronts to the necking site depends on the parabolicity factor: the smaller the n, the higher the velocity of the localization fronts. In this case, the necking rate depends on the tensile strength and the total strain before fracture.

The directional motion of the strain fronts to one localization nucleus and coalescence with it leads to a periodic strain accumulation in it, which is manifested in a faster change of dislocation substructures up to the formation of a fragmented structure during necking.

Thus, the development of plastic deformation is a complex process of self-consistent emergence and motion of localized nuclei of plastic flow. The pattern and dynamics of motion of localized strain nuclei depend greatly on the form of the strain hardening law.

REFERENCES

1. L. B. Zuev and V. I. Danilov, "On the nature of broadscale correlations in plastic flow," *Fiz. Tverd. Tela*, **39**, No. 8, 1399–1403 (1997).
2. L. B. Zuev and V. I. Danilov, "A self-excited wave model of plastic strain," *Philos. Mag. Ser. A.*, **79**, No. 1, 43–57 (1999).
3. L. B. Zuev, I. Yu. Zykov, V. I. Danilov, and S. Yu. Zavodchikov, "Heterogeneity of plastic flow of zirconium alloys with a parabolic law of strain hardening," *Appl. Mekh. Tekh. Fiz.*, **41**, No. 6, 133–138 (2000).
4. A. S. Zaimovskii, A. V. Nikulina, and N. G. Reshetnikov, "*Zirconium Alloys in Nuclear Power Engineering*" [in Russian], Energoatomizdat, Moscow (1994).
5. A. V. Nikulina and V. A. Markelov, "Zr–1%Nb–1% Sn–0.5% Fe alloy for the tubes of high-power reactors," *Vopr. Atom. Nauki Tekh., Ser. Materialoved. Nov. Mat.*, No. 2, 58–66 (1990).

6. T. M. Poletika, L. B. Zuev, and A. A. Nor, "The microstructure of local strain nuclei observed for Zr alloy in the stage of parabolic work hardening," *Appl. Phys., Ser. A.*, **73**, No. 5, 601–603 (2001).
7. T. M. Poletika, G. N. Narimanova, O. V. Gimranova, et al., "Plastic flow localization in Zr–1%Nb alloy," *Z. Tekh. Fiz.*, **72**, No. 9, 57–62 (2002).
8. I. I. Papirov and G. F. Tikhinskii, "Nature of the plastic strain of zirconium," Preprint No. 76-23, Khar'kov Physicotech. Inst., Acad. of Sci. of the UkrSSR, Khar'kov (1976).
9. A. Akhtar and E. Teghtsoonian, "Plastic deformation of zirconium single crystals," *Acta Metall.*, **19**, No. 3, 655–663 (1971).
10. J. E. Bailey, "Electron microscope studies of dislocations in deformed zirconium," *J. Nuclear Mater.*, **7**, No. 1, 300–310 (1962).
11. V. A. Markelov, V. Z. Rafikov, and S. A. Nikulin, "Changes in the microstructure of Zr alloy with Sn, Nb, and Fe under thermal strain," *Fiz. Metal. Metalloved.*, **77**, No. 4, 70–79 (1994).
12. R. Jones and C. Wykes, *Holographic and Speckle Interferometry*, Cambridge Univ. Press, Cambridge, London, New York (1983)).
13. V. I. Trefilov, V. F. Moiseev and É. P. Pechkovskii, *Strain Hardening and Fracture of Polycrystalline Metals* [in Russian], Naukova Dumka, Kiev (1987).
14. D. L. Douglass, *The Metallurgy of Zirconium*, IAEA, Vienna (1971).
15. J. L. Derep, S. Ibrahim, R. Rouby, and G. Fantozzi, "Strain behavior of Zircaloy-4 between 77 and 900 K," *Acta Metall.*, **28**, No. 5, 607–619 (1980).
16. T. P. Chernayeva, A. I. Stukaov, and V. M. Gritsina, "Behavior of oxygen in zirconium," *Vopr. Atom. Nauki Tekh., Ser. Materialoved. Nov. Mat.*, No. 2, 71–85 (1999).
17. É. V. Kozlov, V. A. Starenchenko, and N. A. Koneva, "Evolution of the dislocation substructure and the thermodynamics of plastic deformation in metal materials," *Metally*, No. 5, 152–161 (1993).
18. V. V. Rybin, "Physical model for mechanical instability and necking," *Fiz. Metal. Metalloved.*, **44**, No. 3, 623–632 (1977).
19. R. W. K. Honeykombe, *The Plastic Deformation of Metals*, Edward Arnold, London (1968).
20. A. A. Samarskii, G. G. Elenin, N. V. Zmitrenko, et al., "Combustion of a nonlinear medium in the form of complex structures," *Dokl. Akad. Nauk SSSR*, **237**, No. 6, 1330–1333 (1977).
21. L. B. Zuev and B. S. Semukhin, "Some acoustic properties of a deforming medium," *Philos. Mag. Ser. A.*, **82**, No. 6, 1183–1193 (2002).